

IMPROVED CONFLICTING-DIP TREATMENT IN THE OFFSET-CONTINUATION TRAJECTORY STACK

T. A. Coimbra, A. Novais, and J. Schleicher

email: *js@ime.unicamp.br*

keywords: *Multi-parameter stacking, conflicting dips, velocity analysis*

ABSTRACT

The offset-continuation trajectory (OCT) stack is a multi-parameter stacking technique that allows to construct stacked zero or common-offset sections. Like other multi-parameter stacking techniques, it has difficulties to handle conflicting dips when selecting only one optimal parameter sets. The treatment of conflicting dips can be improved by means of a Feynman-inspired multi-path summation. Using an exponential weight as a function of semblance along the trajectories, the stack is carried out over all possible dips. In this way, all events that produce significant coherence along their associated OCO trajectories will be carried over to the stacked section. Our numerical tests demonstrate that the procedure significantly improves events with conflicting dips in the stacked section.

INTRODUCTION

For data of very low signal-to-noise (S/N) ratio or acquisitions with very low fold, conventional common-midpoint (CMP) processing might not provide stacked sections of sufficient quality. In such situations, alternative processing sequences making use of a higher fold are necessary to improve the data quality. Common-reflection-surface stack (see, e.g., Höcht et al., 1999; Jäger et al., 2001; Hertweck et al., 2007) and multifocusing (Gelchinsky et al., 1999) are such generalized stacking techniques. In the 2012 WIT report, Coimbra et al. (2012b) introduced an alternative technique that also makes use of a higher data fold. This method uses stacking along the event trajectories of the offset-continuation operation (OCO, see Deregowski and Rocca, 1981). Therefore, Coimbra et al. (2012b, 2013) refer to this stacking process as offset-continuation trajectory stack or briefly OCT stack.

The OCT stack represents an alternative path for the processing of reflection-seismic data. Its key element is the construction of stacked sections at any arbitrary offset, together with corresponding coherency sections and sections of kinematic and dynamic wavefield attributes.

The OCT stack makes use of so-called OCO trajectories (Coimbra et al., 2012a). Such a trajectory requires only two parameters (local event slope and stacking velocity) to describe a seismic reflection event in the multi-coverage data. Using these parameters, the method stacks the data along a predicted travelttime curve that approximates the CRP event (Coimbra et al., 2012b). Since the parameters, and thus the predicted travelttime curve, can be updated from the data at each offset, the approximation has the potential of providing better approximations (and thus better stacks) than conventional methods that adjust the approximate travelttime expression only once at some initial point.

One problem of the OCT stack, like all single or multi-parameter stacking methods, is its treatment of conflicting dips. Since generally, one a single parameter value is chosen at a certain starting point, these methods generally have difficulties when two or more events intersect just at the starting point. In this report, we present a method based on Feynman's multi-path idea of how to reduce this kind of problem and come up with stacked sections that contain more information on intersecting events.

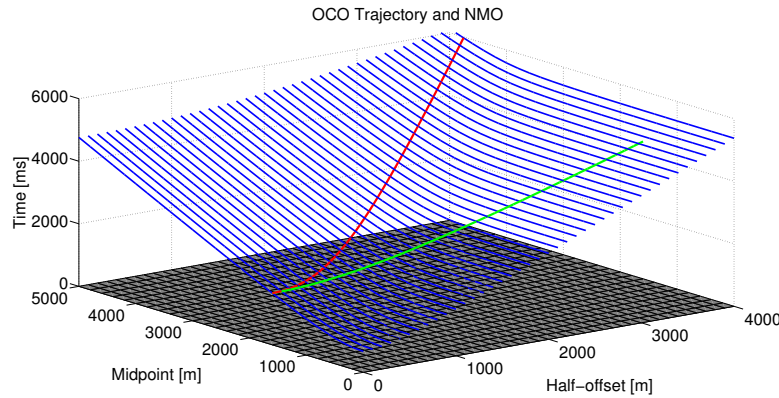


Figure 1: Traveltime surface of a dipping reflector in multi-fold data together with the location of an OCO trajectory (red line) as compared to CMP traveltime curves (green line). The OCO trajectory approximates the position of events reflected at a common reflection point in a medium with average velocity.

THEORETICAL DESCRIPTION

Coimbra et al. (2012b, 2013) derived the theoretical basis for the stack along OCO trajectories, based on the kinematic behaviour of the OCO transformation as described by the OCO image-wave equation (Hubral et al., 1996). Here we briefly summarize the main theoretical ideas.

OCO trajectories

Coimbra et al. (2012a) studied the kinematics of the offset-continuation operation (OCO) and derived the OCO trajectory tracing system by means of applying the method of characteristics to the second-order linear partial differential equation known as the OCO image-wave equation (Hubral et al., 1996). Formally, we can think of the solution to this equation as being approximated by an expression that is analogous to the one used in ray theory, i.e., the leading term of a high-frequency asymptotic (WKB-type) approximation for a reflected wave recorded on a seismogram. Thus, the leading high-frequency term describes the image-wave front for the OCO image wave. In other words, the image-wave front can be thought of as being represented by an OCO eikonal, governed by an image-eikonal equation.

The solution of the OCO eikonal equation leads to ray-like trajectories describing the change of position of a selected point P_0 on a seismic reflection event S_0 in a common-offset section at h_0 when changing the half-offset. The curve in space described by all possible positions of the reflection events of a common reflection point under variation of the half-offset is the so-called OCO trajectory (Coimbra et al., 2012a, see also Figure 1). In other words, an OCO trajectory describes the position of events reflected at the same depth point in all common-offset sections.

The algebraic procedure to construct the OCO trajectories can be summarized as follows. As shown by Coimbra et al. (2012b, 2013), the traveltime surface in the offset-midpoint-time space is a hypersurface $S_H(t, \xi, H) = 0$ (see again Figure 1), where H is the OCO eikonal. It must satisfy

$$H(\xi_h, t_h(\xi_h)) = h, \quad (1)$$

in all common-offset sections. At $h = h_0$, the hypersurface S_H coincides with the reflection event in the common-offset section for h_0 , i.e.,

$$S_0 = S_H(t(h_0, \xi_{h_0}), \xi(h_0, \xi_{h_0}), h_0) = 0. \quad (2)$$

This leads to a family of characteristic curves $t = t(h, \xi_{h_0})$, $\xi = \xi(h, \xi_{h_0})$, and $H = H(h, \xi_{h_0})$, which depend on ξ_{h_0} and h as parameters. Fixing $h = h_0$ and varying ξ_{h_0} we obtain the curve S_0 . On the other hand, fixing ξ_{h_0} and varying h , we obtain the OCO trajectories.

For a medium described by a constant average velocity V , Santos et al. (1997) have demonstrated that for one fixed ξ_{h_0} , all possible OCO trajectories must satisfy

$$t^2 = t(\xi, h; \xi_{h_0}, t_{h_0}, h_0)^2 = \frac{4h^2}{V^2} + \frac{4h^2(t_{h_0}^2 - 4h_0^2/V^2)}{u^2}, \quad (3)$$

with

$$u = \sqrt{(h + h_0)^2 - (\xi - \xi_{h_0})^2} + s\sqrt{(h - h_0)^2 - (\xi - \xi_{h_0})^2}, \quad (4)$$

where $s = \text{sgn}(h - h_0)$. Equation (3) as a function of ξ for a fixed h is also known as the OCO Huygens-image curve. It depends on the parameters ξ , h , ξ_{h_0} , t_{h_0} and h_0 , but is independent of the slope of the event through P_0 . It describes all possible positions in the common-offset section at h of a reflection event that was observed at $P_0 = (\xi_0, t_{h_0})$ in the common-offset section at h_0 .

However, the actual path of the OCO trajectory for a specific reflection event depends on the event slope at P_0 . To describe this dependence, we parameterize $t_{h_0} = t_{h_0}(\xi_{h_0})$ and consider ξ_{h_0} as a function of ξ , h and h_0 . The envelope of all OCO Huygens image-curves for all points on S_0 describes the hypersurface S_H at half-offset h . It is constructed by taking the derivative of t in equation (3) with respect to ξ_{h_0} and setting it to zero. This results in the relationship between the position ξ of the event at half-offset h to its position ξ_{h_0} at h_0 given by

$$\xi = \xi(h; \xi_{h_0}, t_{h_0}, \phi_0, h_0) = \xi_{h_0} + 2\Upsilon_{h_0}(h^2 - h_0^2)/Q, \quad (5)$$

where

$$Q = \sqrt{\Upsilon_{h_0}^2 \eta^2 + 2t_{n_0}^4 + 2\sqrt{t_{n_0}^8 + \Upsilon_{h_0}^2 t_{n_0}^4 \eta^2 + 16\Upsilon_{h_0}^4 h^2 h_0^2}}. \quad (6)$$

Here,

$$t_{n_0} = \sqrt{t_{h_0}^2 - 4h_0^2/V^2} \quad (7)$$

is the NMO corrected travelttime at the initial half-offset h_0 ,

$$\eta = 2\sqrt{h^2 + h_0^2} \quad (8)$$

is twice the geometric mean of half-offsets h and h_0 , and

$$\Upsilon_{h_0} = t_{h_0} \phi_0, \quad (9)$$

with ϕ_0 denoting the dip of the reflection event S_0 at P_0 .

Together, equations (3) and (5) constitute a parametric form of the hypersurface S_H . For a fixed ξ_{h_0} these equations thus describe the OCO trajectory from P_0 to any other common-offset at h . In other words, equations (3) and (5) represent the position of events that are reflected at the same point in depth (if the medium was exactly described by the OCO velocity V), i.e., the OCO trajectory belongs to a common-reflection point (CRP).

The OCO trajectory starting at some initial half-offset $h_0 = h_i \neq 0$ and ending at the final half-offset $h = 0$ can be alternatively described in the opposite direction as starting as $h_0 = 0$ and ending at h_i . Thus, their midpoint dislocations $\xi_0 - \xi$ must be the same, except for their sign. This leads to the relationship between the event slopes in the $\text{CO}(h_0)$ and $\text{CO}(h)$ sections given by

$$\phi = \phi_0 \frac{t_n^2 t_{h_0}}{t_{n_0}^2 t}, \quad (10)$$

where

$$t_n = \sqrt{t^2 - 4h^2/V^2} \quad (11)$$

is the NMO corrected travelttime at half-offset h .

STACK ALONG OCO TRAJECTORIES

The OCO trajectories can be used to approximate the travelttime surface using the set of equations (3), (5), and (10). Along the best-fitting trajectories, the data can be stacked in a similar manner to conventional stacking techniques.

The best-fitting OCO trajectories are found as follows: For a central point P_0 with coordinates $(\xi_{h_0}, t_{h_0}, h_0)$, we trace trial OCO trajectories for each possible combination of values for V and ϕ_0 . The pair that provides the highest coherence along the trial trajectory defines the OCO trajectory for P_0 . Of

course, a more efficient algorithm should involve some optimization technique in the search for the best parameter pair.

To incorporate information about the time dip in the direction perpendicular to the trial trajectories, the coherence is evaluated not only along the OCO trajectory, but also along the dip direction in a small window of neighboring traces (7 traces in our implementation) around the trajectory. In symbols, the stacking surface can be represented as

$$\tau(\xi_n, h; \xi_{h_0}, t_{h_0}, h_0) = t(\xi, h; \xi_{h_0}, t_{h_0}, h_0) + \phi(\xi_n - \xi), \quad (12)$$

where t and ξ are given by equations (3) and (5), and where $\xi_n = \xi + n\Delta\xi$ is the location of the n th neighboring trace in the common-offset section at h . Moreover, ϕ denotes the local event dip at the OCO trajectory in the common-offset section at h . It is determined at each half-offset from its initial value ϕ_0 by means of equation (10).

Denoting the parameter pair of local event dip ϕ_0 and average velocity V for the so-determined best-fitting OCO trajectory as $\Xi = (\phi_0, V)$ to simplify the notation, the OCT stack between half-offsets h_0 and h_f can be written as

$$M(P_0; \Xi, h_f) = \sum_{h=h_0}^{h_f} \sum_{n=-N}^N U(\xi_n, \tau(\xi_n, h; \xi_{h_0}, t_{h_0}, h_0; \Xi), h), \quad (13)$$

where $U = U(\xi, t, h)$ is reflection seismic data in the midpoint-time-offset domain and N (3 in our implementation) is number of traces to each side of the principal trace that define the dip window.

Conflicting dips

Choosing only the parameter pair $\Xi = (\phi_0, V)$ that produces the highest coherence will lead to suppressed events when two or more of them are intersecting at the central point P_0 . The stacking procedure can be modified to improve the treatment of conflicting dips. In this work, we used a Feynman-inspired multi-path summation technique similar to the one applied by Landa et al. (2006) for imaging. For this purpose, we calculate the coherence-weighted average over all stacking results for different dips obtained with the same mean velocity V that provided the best-fitting OCO trajectories. In symbols,

$$M_s(P_0) = \langle M(P_0, \Xi) \rangle_V = \int_{\phi_1}^{\phi_2} C_M(P_0, \Xi) M(P_0; \Xi, h) d\phi_0, \quad (14)$$

where C_M is a coherence measure. In our implementation, we used an exponential weight function of the form

$$C_M(P_0, \Xi) = \frac{1}{\bar{C}_M} \exp \left\{ \left[1 - \frac{1}{S_T(\Xi)} \right] \alpha \right\} \frac{1}{S_T(\Xi)}, \quad (15)$$

where $S_T(\Xi)$ is the normalized semblance (Neidell and Taner, 1971) along the OCO trajectory described by the parameter pair $\Xi = (\phi_0, V)$ and \bar{C}_M is a normalization factor. Parameter α controls the shape of the exponential weight function. Figure 2 shows one side of the symmetrical weight function C_M for two values of α . For a single event, the normalization factor should be

$$\bar{C}_M = \int_{\phi_1}^{\phi_2} C_M(P_0, \Xi) d\phi_0, \quad (16)$$

but for conflicting events, it is an estimate of the area below a single coherence peak.

To justify the choice of the above weight function, let us consider two events with conflicting dips at some initial point P_0 . Then, the semblance S_T as a function of ϕ_0 will have two coherence peaks as indicated in Figure 3. The optimal velocity parameter value for both events should be identical or very close, because it represents the average medium velocity at that midpoint and half-offset.

To an integral of the form of equation (14), we can apply Laplace's Method (Olver, 1974; Bleistein and Handelsman, 1986). It says that for large values of α , such integrals can be asymptotically approximated

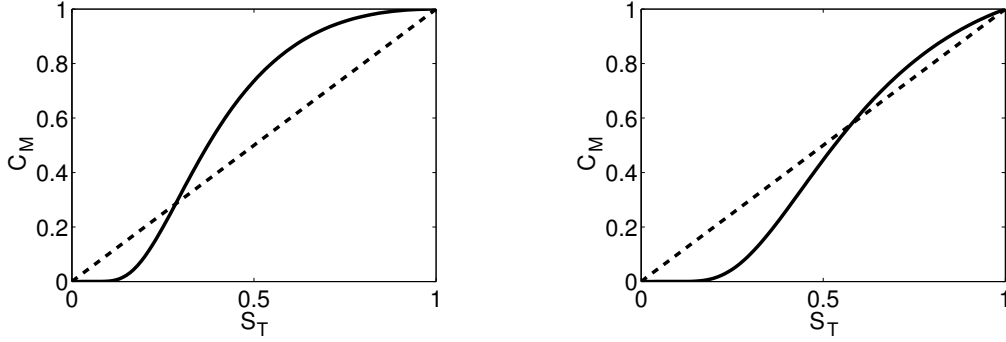


Figure 2: Weight function C_M for the OCT stack as a function of normalized semblance S_T with (a) $\alpha = 1$, (b) $\alpha = 1.5$.

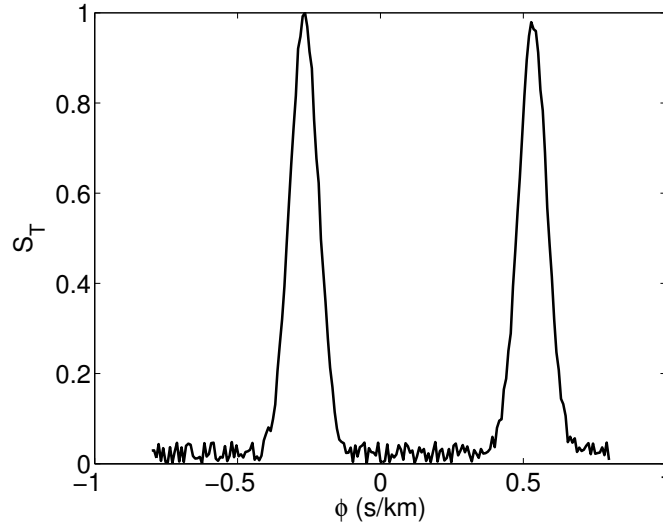


Figure 3: Coherence S_T as a function of dip parameter ϕ_0 for two events with conflicting dip at P_0 .

by

$$\int_R g(x)e^{\alpha L(x)} dx \approx \sum_{j=1}^N A_j e^{\alpha L(x_j)}, \quad (17)$$

where the points x_j are the stationary points inside the integration domain R , i.e., those points where the derivative of the function $L(x)$ vanishes, as long as the second derivatives of $L(x)$ at all points x_j are negative, i.e., all the stationary points represent local maxima. The factor

$$A_j = g(x_j) \sqrt{\frac{2\pi}{\alpha}} \left| \frac{d^2 L}{dx^2} \right|_{x_j}^{-1/2} \quad (18)$$

represents an estimate of the area below the function in the region of the stationary point x_j .

Application of Laplace's Method to integral (14) yields for our two conflicting events

$$M_s(P_0) \approx \left(S_1 \frac{A_1 e^{\alpha \left(1 - \frac{1}{S_T(\phi_1)}\right)}}{C_M} + S_2 \frac{A_2 e^{\alpha \left(1 - \frac{1}{S_T(\phi_2)}\right)}}{C_M} \right). \quad (19)$$

where we have denoted the individual unweighted OCT stacking results along the two OCO trajectories with optimal parameter pairs Ξ_1 and Ξ_2 by S_1 and S_2 , respectively. Under the assumption that the areas

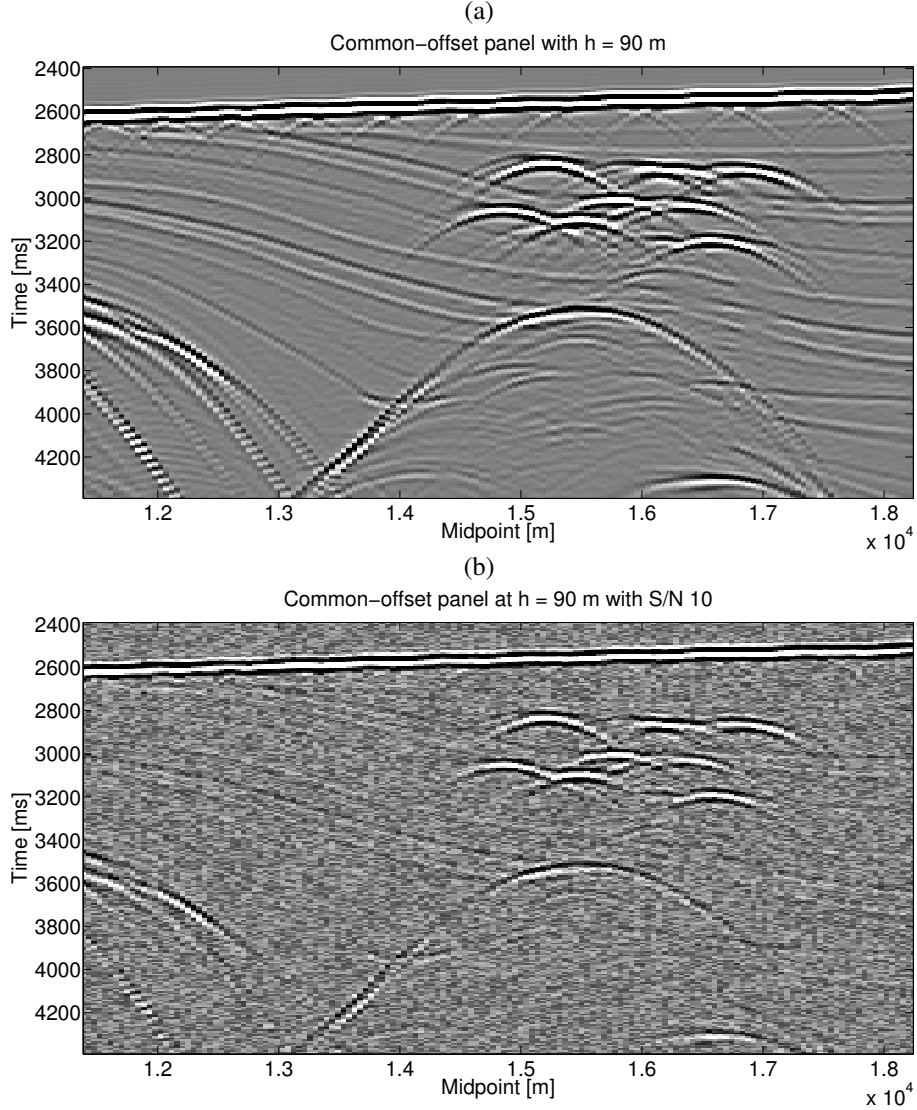


Figure 4: (a) CO section at $h = 90$ m for synthetic test of stacking along OCO trajectories, (b) Noisy reference CO section ($S/N=10$).

under both peaks are well-estimated by \bar{C}_M , i.e., $A_1 \approx A_2 \approx \bar{C}_M$, as well as that

$$\exp(\alpha(1 - 1/S_T(\phi_2))) \approx \exp(\alpha(1 - 1/S_T(\phi_1))) \approx 1, \quad (20)$$

which is exactly true if the normalized semblances S_T at both peaks are equal to one, this reduces to

$$M_s(P_0) \approx S_1 + S_2, \quad (21)$$

which means that the complete stack result along both OCO trajectories is carried over to the final stacked section. This result can be immediately generalized to more than two events with conflicting dips. It remains valid as long as the semblance peaks are not too different.

NUMERICAL RESULTS

To test the OCT stacking technique as described above, we have applied it to a synthetic multi-coverage data set, being a noise-contaminated subset of the Sigsbee2B data. Figure 4a shows a common-offset section for $h = 90$ m of the used part of the original Sigsbee2B data, and Figure 4b shows the corresponding noisy section with random noise with a S/N ratio of 10.

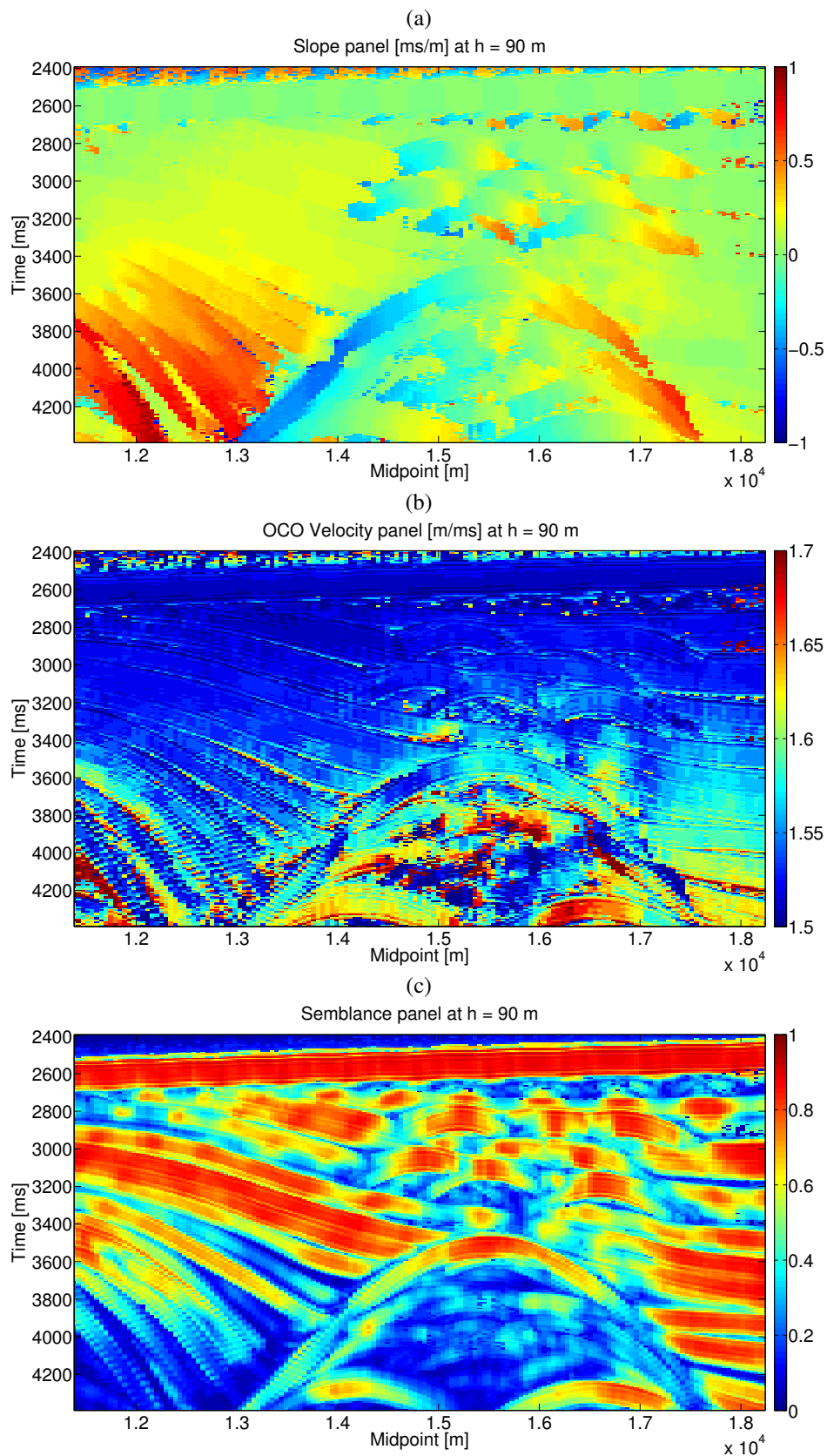


Figure 5: (a) Traveltime slope of the major coherence, (b) OCO velocity panel. (c) Semblance along OCO trajectory of the major coherence.

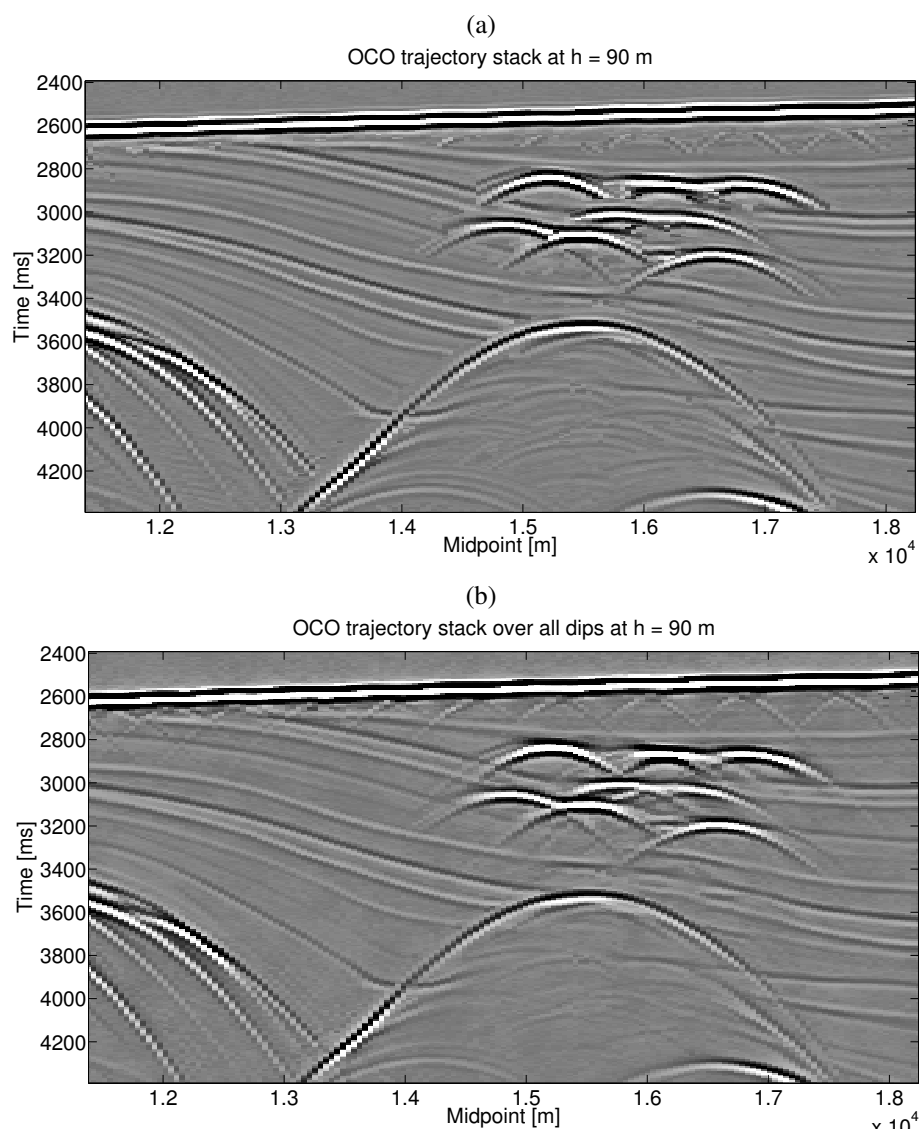


Figure 6: (a) Initial OCT stacked section with only one parameter pair per data point. (b) Final OCT stacked section with improved treatment of conflicting dips.

Figures 5-7 illustrate the procedure. For each point in the reference CO section for $h = 90$ m (Figure 4a), we applied the OCT stack to the noisy multi-coverage data. The maximum semblance (Figure 5c) along all trial OCO trajectory determines the parameter pair of traveltime slope (Figure 5a) and OCO velocity (Figure 5b) that define the best-fitting OCO trajectory through the multi-coverage data.

The result of the stack using these values according to equation 13 is a noise-attenuated stacked CO section (Figure 6a) corresponding to the reference section (which may, but need not exist among the acquired data). We observe a strong noise reduction in comparison to the noisy data section in Figure 4b. All strong events are nicely recovered. Even most of the events that are barely or not visible in the noisy section of Figure 4b are present in the stacked section. However, as expected, wherever there are events with conflicting dips in the original data section of Figure 4a, the weaker events are suppressed.

Figure 6b shows the result of the coherence-weighted average of all stacking results for the best velocity but all possible event slopes according to equation 14. We immediately recognize that this procedure improves the treatment of conflicting dips. Particularly the diffraction events in the upper part of the section, but also other events with conflicting dips, are strongly improved as compared to Figure 6a. A drawback of the weighted procedure is that weaker events, which produce lower coherence values (such as

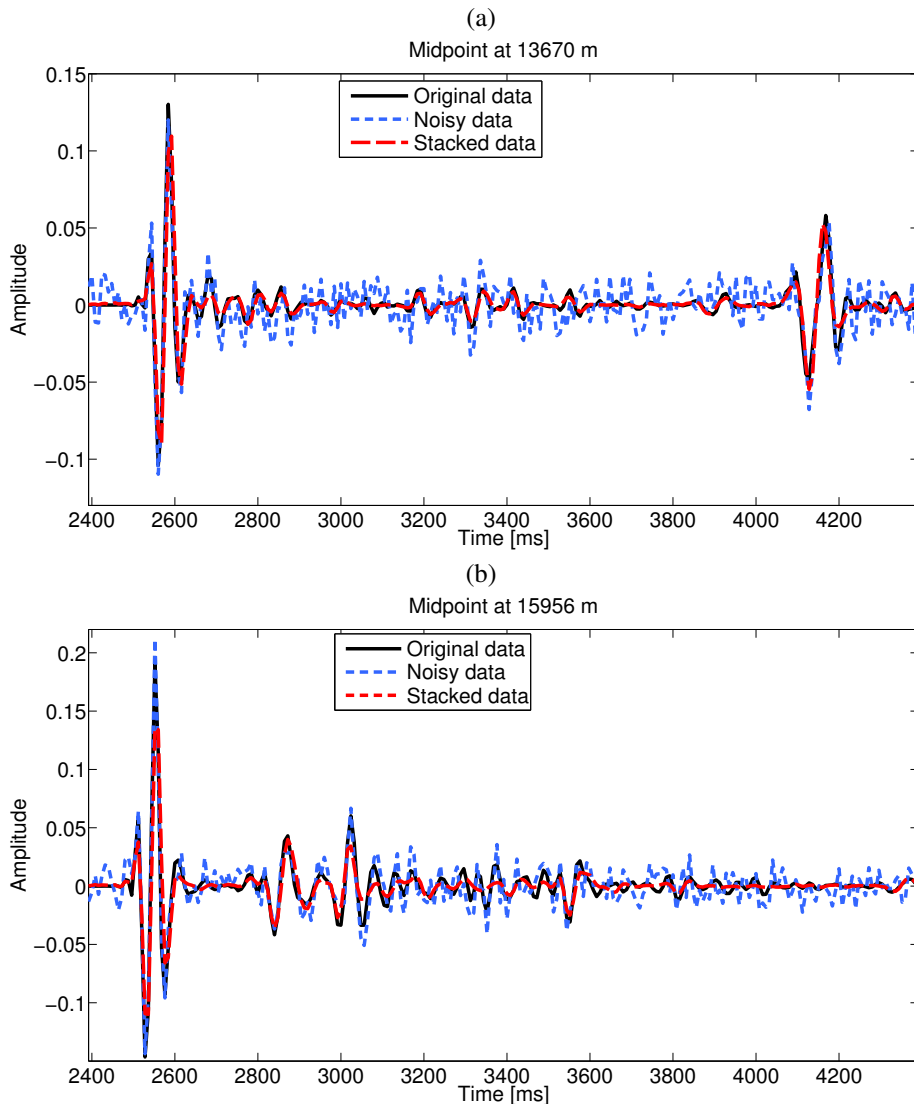


Figure 7: Comparison between original (black, solid), noisy (blue, short dashes), and stacked (red, long dashes) traces at two midpoint locations: (a) $\xi_{h_0} = 13.670$ km, (b) $\xi_{h_0} = 15.956$ km.

the events in the central lower part of the data section) are further reduced by the coherence weight.

Figure 7 shows a trace-to-trace comparison of the original noise-free Sigsbee2B data, the corresponding noisy data, and the coherence-weighted OCT stacked section at two midpoint positions. The first trace (Figure 7a) is the one at $\xi_{h_0} = 13.670$ km in a region without strong diffraction events. We see that the stacked traces recover the original traces almost perfectly. At the second midpoint position at $\xi_{h_0} = 15.956$ km, there are several diffraction events visible in the data at times between 2.8 s and 3.2 s. We see that in this time interval, almost all events are also recovered with high quality. However, while all arrivals are present in the OCT-stacked data, some of the later arrivals with small amplitudes are further reduced.

Finally, the knowledge of the best possible OCO trajectories for each point in the stacked data section allows to construct well-approximated CRP gathers. Parts b and c of Figure 8 compare a conventional CMP gather with a CRP gather obtained by selecting data along OCO trajectories for points at the midpoint and in the time interval indicated by a solid black line in the data section of Figure 8a. While the flatness of both gathers is comparable, it is to be noted that only the events in the CRP gather can be thought of as stemming from approximately the same reflection points. This leads to visible amplitude differences between the two gathers. For example, within the circles in Figure 8b and c we see that there exists a significant difference between amplitudes of both data along certain events, indicating that an AVO analysis in the CRP section

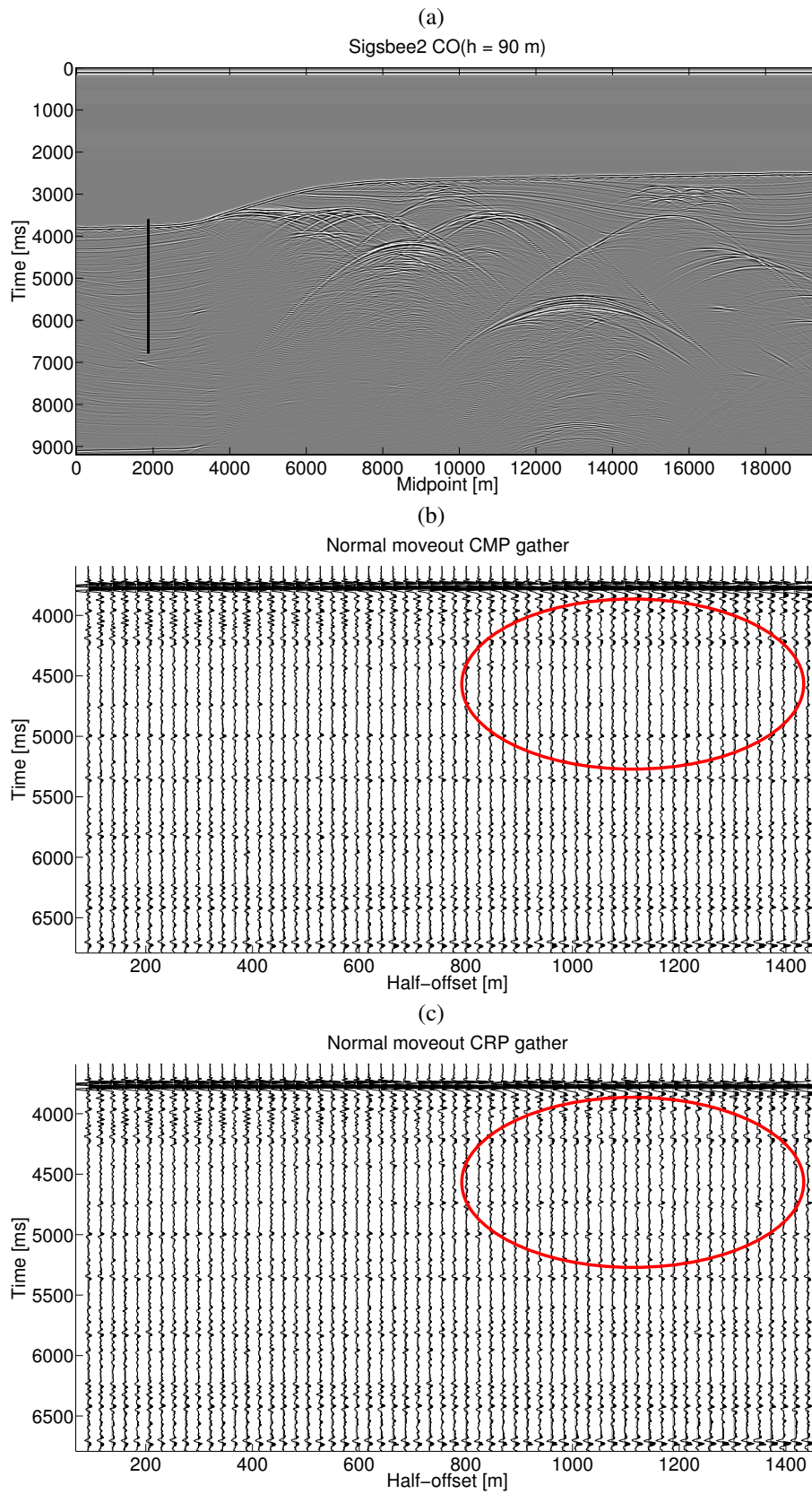


Figure 8: (a) Sigsbee2B data near-offset section, (b) Normal moveout CMP panel. (c) Normal moveout CRP panel.

would provide different (and probably improved) results over those from the CMP section.

DISCUSSION

OCO trajectories (Coimbra et al., 2012a) can be used for a multi-parameter stacking procedure similar to its relatives, the CMP and CRS stacks and multifocusing. By stacking along trial trajectories, the OCO trajectory (OCT) stack (Coimbra et al., 2012b) automatically determines stacking attributes based on a coherence measure applied at every common-offset sample of the data. The main advantages of the OCO trajectories are twofold. Firstly, in comparison to a CMP or zero-offset CRS stack, the procedure is not limited to a zero-offset stacked section. This allows for the construction of stacked common-offset sections to improve the signal-to-noise ratio or even to interpolate the data. Secondly, in comparison to an offset CRS stack, the OCO trajectory stack needs less parameters to construct the stacked CO sections. In the 2D/2.5D case as discussed here, only two parameters (stacking velocity and local traveltime slope) are needed.

CONCLUSIONS

We have developed a new method to improved the treatment of conflicting dips in the offset-continuation trajectory (OCT) stack. The OCT stack is a multi-parameter stacking technique that allows to construct stacked zero or common-offset sections. The method uses the tracing of offset continuation (OCO) trajectories. These trajectories describe the position of a selected point on a seismic reflection event as a function of offset. By extending the OCO trajectories linearly along the predicted dip direction, they form a stacking surface along which the data can be summed up. In this way, stacked common-offset sections can be constructed for any arbitrary offset. For 2D multi-coverage data, an OCO trajectory is described by only two parameters, being an average velocity that is an approximation to RMS velocity, and the local event slope in the final stacked section.

The new conflicting-dip treatment is based on a Feynman-inspired multi-path summation idea. Using an exponential weight as a function of semblance along the trajectories, the stack is carried out over all possible dips. In this way, all events that produce significant coherence along their associated OCO trajectories will be carried over to the stacked section. Our numerical tests have demonstrated that the procedure significantly improves events with conflicting dips in the stacked section. Though we have tested the procedure with the OCT stack, it is applicable correspondingly to other multi-parameter stacking methods like the CRS stack.

ACKNOWLEDGEMENTS

This work was kindly supported by the Brazilian agencies CAPES, FINEP, and CNPq, as well as Petrobras and the sponsors of the *Wave Inversion Technology (WIT) Consortium*. We specially thank the SMAART-JV for providing the Sigsbee2B_nfs data and model.

REFERENCES

- Bleistein, N. and Handelsman, R. A. (1986). *Asymptotic Expansions of Integrals*. The advanced book program. Dove publications, Inc.
- Coimbra, T. A., Novais, A., and Schleicher, J. (2012a). Offset continuation (OCO) ray tracing using OCO trajectories. *Stud. Geophys. Geod.*, 56:65–82.
- Coimbra, T. A., Novais, A., and Schleicher, J. (2012b). Offset-continuation stacking. *Annual WIT Report*, 15:59–72.
- Coimbra, T. A., Novais, A., and Schleicher, J. (2013). Stacking on OCO trajectories. In *Expanded Abstracts*, pages Th-02-06:1–4. 75th EAGE Meeting.
- Deregowski, S. M. and Rocca, F. (1981). Geometrical optics and wave theory of constant offset sections in layered media. *Geophysical Prospecting*, 29:374–406.

- Gelchinsky, B., Berkovitch, A., and Keydar, S. (1999). Multifocusing homeomorphic imaging - Part 1. Basic concepts and formulas. *Journal of Applied Geophysics*, 75:229–242.
- Hertweck, T., Schleicher, J., and Mann, J. (2007). Data stacking beyond CMP. *The Leading Edge*, 26(7):818–827.
- Höcht, G., de Bazelaire, E., Majer, P., and Hubral, P. (1999). Seismics and optics: hyperbolae and curvatures. *J. Appl. Geoph.*, 42(3/4):261–281. Special Issue on "Macro-Model Independent Seismic Reflection Imaging".
- Hubral, P., Tygel, M., and Schleicher, J. (1996). Seismic image waves. *Geoph. J. Int.*, 125:431–442.
- Jäger, R., Mann, J., Höcht, G., and Hubral, P. (2001). Common- reflection-surface stack: Image and attributes. *Geophysics*, 66:97–109.
- Landa, E., Fomel, S., and Moser, T. J. (2006). Path-integral seismic imaging. *Geophysical Prospecting*, 54(5):491–503.
- Neidell, N. and Taner, M. T. (1971). Semblance and other coherency measures for multichannel data. *Geophysics*, 36:482–497.
- Olver, F. W. J. (1974). *Asymptotics and Special Functions*. Academic Press, Inc.
- Santos, L., Scheicher, J., and Tygel, M. (1997). 2.5-D true-amplitude offset continuation. *J. Seism. Expl.*, 6:103–116.